Radiation Report

OPA4H014-SEP Single-Event Effects (SEE) Radiation Report

ABSTRACT

Studies were performed to characterize the effects of heavy-ion irradiation on the single-event latch-up (SEL) performance of the OPA4H014-SEP precision quad-channel operational amplifier. For device qualification, heavy ions with an LET_{EFF} of 43MeV-cm^2 / mg were used to irradiate the devices with a fluence of 1 × 10^7 ions / cm^2. The results demonstrated that the OPA4H014-SEP is SEL-free up to the specified surface LET_{EFF} = 43MeV-cm^2/ mg at 125°C.

Characterization of single-event transients (SET) and correlation testing of SEL were also performed, up to a surface LET_{EFF} = 50MeV-cm^2/ mg at 125°C. These results suggest the device has additional margin beyond the specified surface LET_{EFF} = 43MeV-cm^2/ mg at 125°C.

Table of Contents

Trademarks

All trademarks are the property of their respective owners.

1 Overview

The OPA4H014-SEP is a low-power JFET input operational amplifier (op amp) that features good drift and low input bias current. With an input range that includes V– and a rail-to-rail output, designers can take advantage of the low-noise characteristics of JFET amplifiers while interfacing to single-supply, precision analog-to-digital converters (ADCs) and digital-to-analog converters (DACs). The OPA4H014-SEP achieves 11MHz unity-gain bandwidth and 20V/µs slew rate, and consumes only 1.8mA (typical) of quiescent current. This device runs on a single 4.5V to 18V supply or dual ±2.25V to ±9V supplies.

Table 1-1. Overview Information(1)

Description	Device Information
TI Part Number	OPA4H014-SEP
MLS Number	OPA4H014PWSEP
DLA VID	V62/21607
Device Function	11MHz, Precision, Low-Noise, RRO, JFET Amp in Space-Enhanced Plastic
Fab Technology	BICMOS
Fab Process	BICOM-3XHV
Exposure Facilities	Radiation Effects Facility, Cyclotron Institute, Texas A&M University Single Event Effects Facility, Facility for Rare Isotope Beams, Michigan State University
Heavy Ion Fluence per Run	1×10^7 ions/cm^2
Irradiation Temperature	125°C (for SEL testing)

(1) TI may provide technical, applications or design advice, quality characterization, and reliability data or service, providing these items shall not expand or otherwise affect TI's warranties as set forth in the Texas Instruments Incorporated Standard Terms and Conditions of Sale for Semiconductor Products and no obligation or liability shall arise from Semiconductor Products and no obligation or liability shall arise from TI's provision of such items.

2 SEE Mechanisms

The primary single-event effect (SEE) of interest in the OPA4H014-SEP is single-event latch-up (SEL). From a risk and potential impact point-of-view, the occurrence of an SEL is possibly the most destructive SEE event and the biggest concern for space applications. A BICMOS process node was used for the OPA4H014-SEP, though the device itself is primarily bipolar. CMOS circuitry introduces a potential for SEL susceptibility. SEL can occur if excess current injection caused by the passage of an energetic ion is high enough to trigger the formation of a parasitic cross-coupled PNP and NPN bipolar structure (formed between the p-sub and n-well and n+ and p+ contacts). The parasitic bipolar structure initiated by a single-event creates a high-conductance path (inducing a steady-state current that is typically orders of magnitude higher than the normal operating current) between power and ground that persists (is *latched*) until the power is removed or until the device is destroyed by the high-current state.

The OPA4H014-SEP is specified as SEL-free to a surface LET_{EFF} of 43MeV-cm^2/ mg, at a fluence of 10^7 ions / cm^2 and a chip temperature of 125°C. The process modifications applied for SEL-mitigation were proven sufficient as the OPA4H014-SEP was shown in characterization to exhibit no SEL with heavy ions up to a surface LET_{EFF} of 50MeV-cm^2/ mg, at a fluence of 10^7 ions / cm^2 and a chip temperature of 125°C.

3 Irradiation Facilities and Telemetry

The heavy ion species used for the SEL qualification studies, and for additional SEL and SET characterization, were provided and delivered by the TAMU Cyclotron Radiation Effects Facility[3] using a superconducting cyclotron and advanced electron cyclotron resonance (ECR) ion source. Ion beams are delivered with high uniformity over a 1-inch diameter circular cross sectional area for the in-air station. Uniformity is achieved by magnetic defocusing. The intensity of the beam is regulated over a broad range spanning several orders of magnitude. For the bulk of these studies, nominal ion fluxes of 1×10^5 ions / s-cm^2 or 5×10^5 ions / s-cm^2 were used to provide heavy ion fluences to 10^7 ions / cm^2.

For correlation SEL and SET testing, heavy ion species were provided and delivered by the MSU Facility for Rare Isotope Beams[4] using a linear particle accelerator ion source. Ion beams were delivered with high uniformity over a 17mm × 18mm area for the in-air station. A current-based measurement is performed on the collimating slits, which intercept 90-95% of the total beam, and this measurement is cross-calibrated against Faraday cup readings. These measurements are real-time continuous and establish dosimetry and integrated fluence. In-vacuum and in-air scintillating viewers are used for measurement of the beam size and distribution. An ion flux of 10^5 ions / s-cm^2 was used to provide heavy ion fluences to 10^7 ions / cm^2.

4 Test Device and Test Board Information

The OPA4H014-SEP is packaged in an 14-pin TSSOP package. Figure 4-1 shows the pinout diagram.

The package was decapped to reveal the die face for all heavy ion testing.

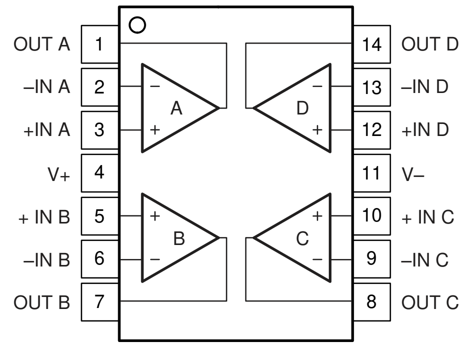

Figure 4-1. OPA4H014-SEP Pinout Diagram

4.1 Qualification Devices and Test Board

The OPA4H014-SEP was biased in a buffer condition, where V+ was set to 9V and V- was set to -9V. On all four channels, the inverting input was connected to the output and the non-inverting input was grounded to midsupply. Current was monitored over time for both V+ and V-. Heavy ions with LET_{EFF} = 43MeV-cm^2 / mg were used to irradiate the devices. A nominal flux of 10^5 ions / s-cm^2 and fluence of 10^7 ions / cm^2 were used during the exposure at 125°C. Two runs were completed to provide an overall fluence of 2 × 10^7 ions / cm^2.

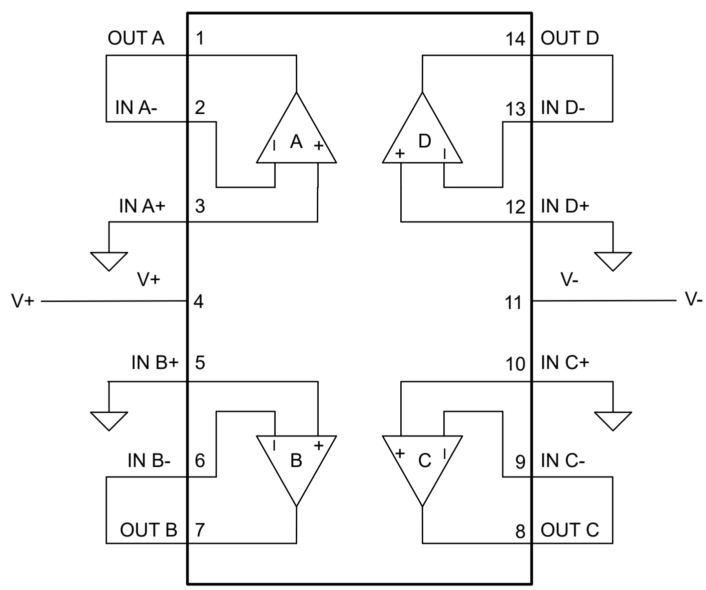

Figure 4-2. OPA4H014-SEP SEL Qualification Bias Diagram

4.2 Characterization Devices and Test Boards

Heavy ions were used to irradiate the devices. A nominal flux of 1 × 10^5 ions / s-cm^2 was used for SEL characterization, at 125°C die temperature. Nominal fluxes of 1 × 10^5 ions / s-cm^2 to 5 × 10^5 ions / s-cm^2 were used for SET characterization, at ambient temperature.

For SEE characterization, the OPA4H014-SEP was biased with split supplies. On all four channels, the inverting input was connected to the output as shown in Figure 4-3. Both a buffer condition and positive-gain condition were tested. Jumpers were used to modify the load resistance and change from G = 1 to G = 10. The default positions are shown.

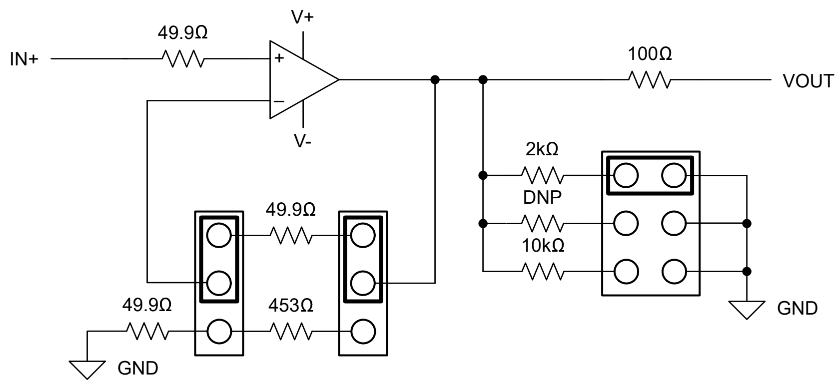

Figure 4-3. SEE Characterization Board Schematic

Input and supply voltages were provided by SMU PXI cards, connected with banana cables. A common input signal was applied to all channels. Figure 4-4 shows the decoupling capacitance scheme used on each board. Current was monitored over time for both V+ and V-. For SET testing, the device outputs were monitored using oscilloscope PXI cards, connected with BNC cables. 100Ω of series isolation resistance was used on each output channel to drive the cable capacitance.

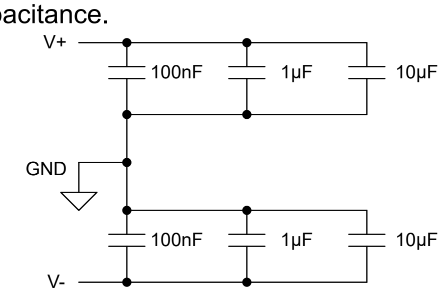

Figure 4-4. Characterization Board Decoupling Capacitances

An example of a decapped unit mounted on a characterization board is shown in Figure 4-5. The back side of the characterization board is shown in Figure 4-6. Note that despite silkscreen marking, 2kΩ resistors were used instead of 50Ω.

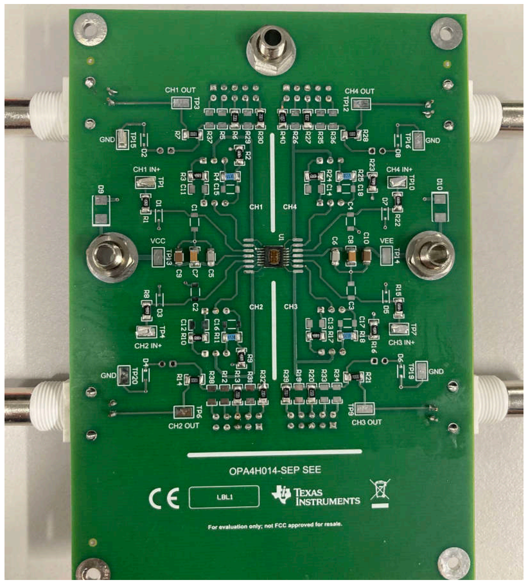

Figure 4-5. Characterization Board (Front)

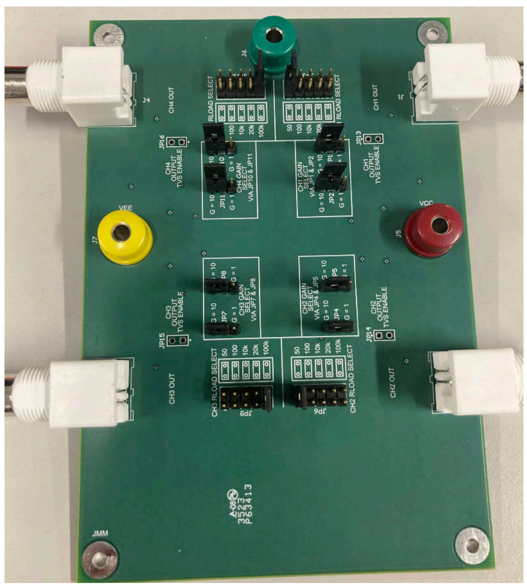

Figure 4-6. Characterization Board (Back)

5 Results

5.1 SEL Qualification Results

During SEL qualification, the device was heated using forced hot air, maintaining an IC temperature at 125°C. The temperature was monitored by means of a K-type thermocouple attached as close to the device as possible. The species used for the SEL testing was a silver (^{47}Ag) ion with an angle-of-incidence of 0° for an LET_{EFF} = 43MeV-cm^2/mg. The kinetic energy in the vacuum for this ion is 1.634 GeV (15MeV/amu line). A flux of approximately 10^5 ions / cm^2-s and a fluence of approximately 10^7 ions were used for two runs. The V+/V-supply voltage was supplied at the recommended maximum voltage setting of +/- 9V. Run duration to achieve this fluence was approximately two minutes. No SEL events were observed during all four runs listed in Table 5-1. Figure 5-1 shows a plot of the current versus time.

Table 5-1. OPA4H014-SEP SEL Conditions Using ^{47}Ag at an Angle-of-Incidence of 0°

Run #	Distance (mm)	Temperature (°C)	Ion	Angle	Flux (ions × cm^2/mg)	Fluence (Number ions)	LET_{EFF} (MeV × cm^2/ mg)
6	40	125	Ag	0°	1.00E+05	1.00E+07	43
7	40	125	Ag	0°	1.00E+05	1.00E+07	43

No SEL events were observed, which indicates that the OPA4H014-SEP is SEL-immune at LET_{EFF} = 43MeV-cm^2/ mg and T = 125°C. Using the MFTF method described in Appendix C and combining (or summing) the fluences of the two runs at 125°C (2 × 10^7), the upper-bound cross-section (using a 95% confidence level) is calculated in Equation 1:

$$\sigma SEL \le 1.84 \times 10^{-7}\ cm^2 \text{ for } LET_{EFF} = 43MeV\text{-}cm^2/\ mg \text{ and } T = 125°C. \quad (1)$$

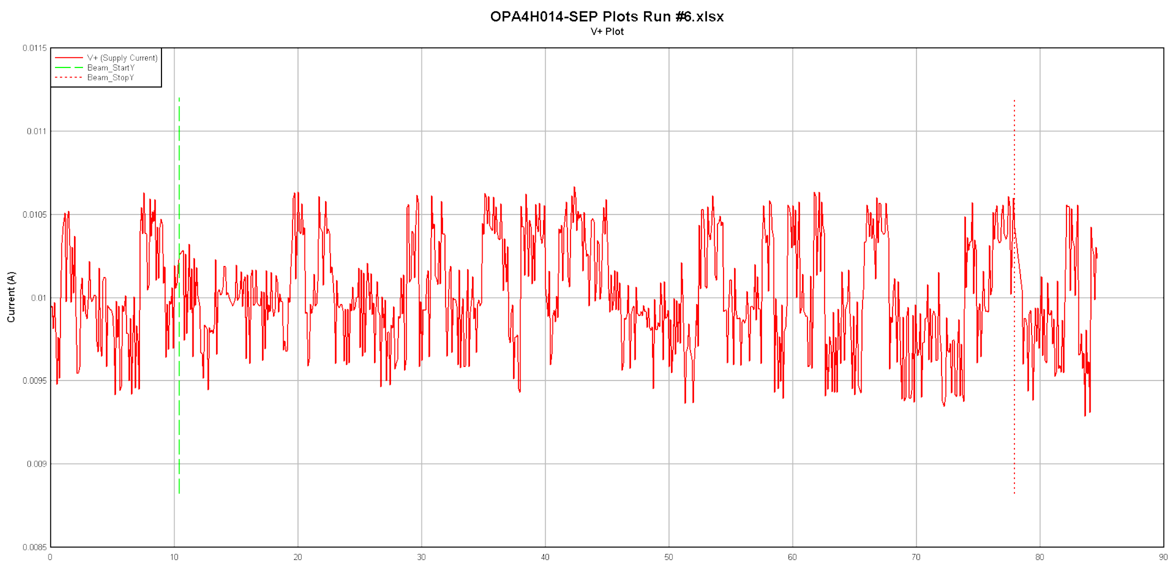

Figure 5-1. Current vs Time (I vs t) Data for V+ Current During SEL Run 6

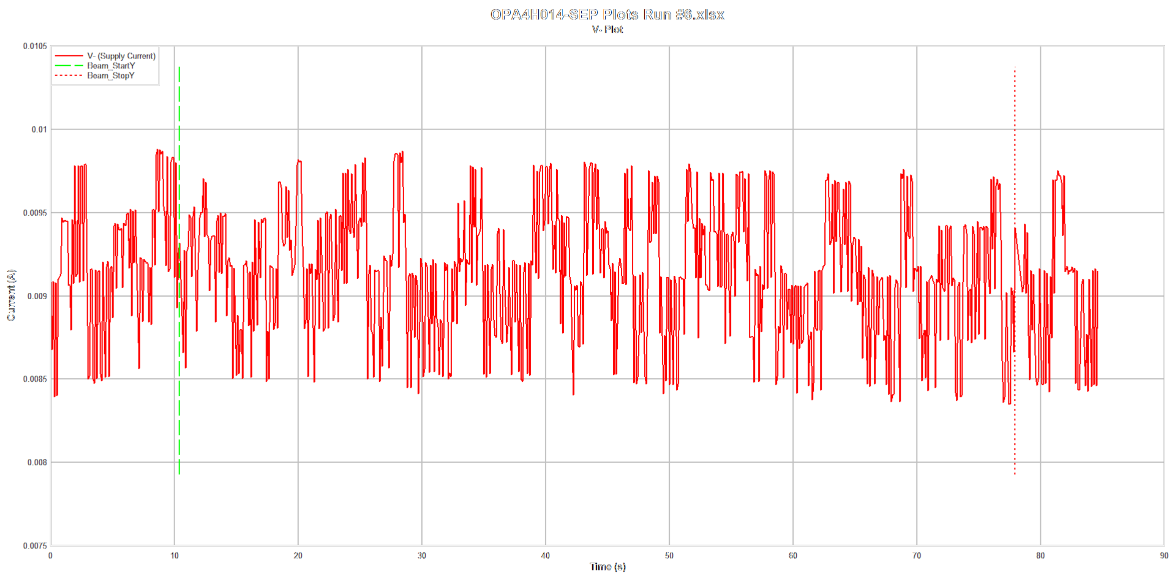

Figure 5-2. Current vs Time (I vs t) Data for V- Current During SEL Run 6

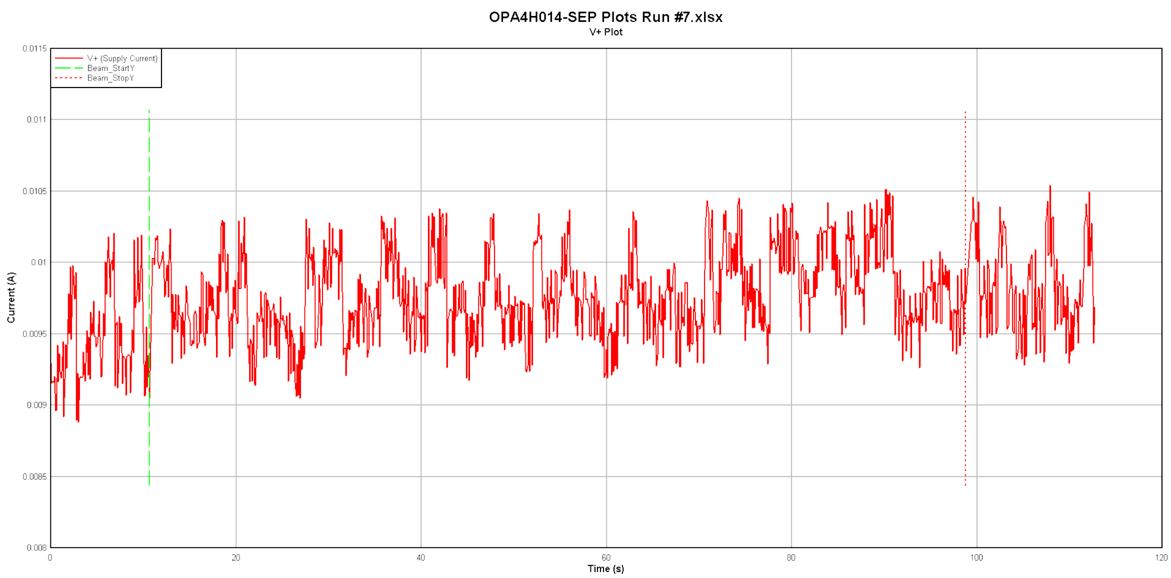

Figure 5-3. Current vs Time (I vs t) Data for V+ Current During SEL Run 7

Figure 5-4. Current vs Time (I vs t) Data for V- Current During SEL Run 7

5.2 SET Characterization Results: TAMU K500 Cyclotron

Two fresh DUTs were used for follow-up SEL characterization. The die temperature of each was held at 125°C as the units were exposed to an ion stream of ^{109}Ag, for a nominal surface LET of 44.8MeV-cm^2 /mg (Bragg peak approximately 59.4MeV-cm^2 /mg). A nominal flux of 10^5 ions / s-cm^2 was used, with each run concluding once a fluence of 10^7ions/cm^2 was reached. Each DUT was tested at both maximum and minimum supply voltages, and in both buffer and positive-gain circuit configurations, with an input signal of V_{IN} = 1V for buffer circuits and V_{IN} = 0.1V for positive-gain circuits. Each output channel was loaded with a 2kΩ resistance to GND (midsupply). No latchup was observed for either DUT under any of the test conditions.

Table 5-2. TAMU SEL Characterization Run Summary

Run Number	DUT	Die Temperature (°C)	Ion	LETeff (MeV-cm^2 /mg)	Flux (ions/s-cm^2)	Fluence (ions/cm^2)	Total Ionizing Dose (rad)	V_S (V+ − V-)	Gain
1	1	125	^{109}Ag	44.8	9.717×10^4	1.001×10^7	7187	4.5	1
2	1	125	^{109}Ag	44.8	1.005×10^5	1.003×10^7	7203	18	1
3	1	125	^{109}Ag	44.8	1.028×10^5	9.963×10^6	7156	4.5	10
4	1	125	^{109}Ag	44.8	1.002×10^5	9.974×10^6	7164	18	10
5	2	125	^{109}Ag	44.8	1.015×10^5	9.991×10^6	7176	4.5	1
6	2	125	^{109}Ag	44.8	1.011×10^5	1.004×10^7	7209	18	1
7	2	125	^{109}Ag	44.8	1.008×10^5	9.991×10^6	7176	4.5	10
8	2	125	^{109}Ag	44.8	1.046×10^5	1.002×10^7	7195	18	10

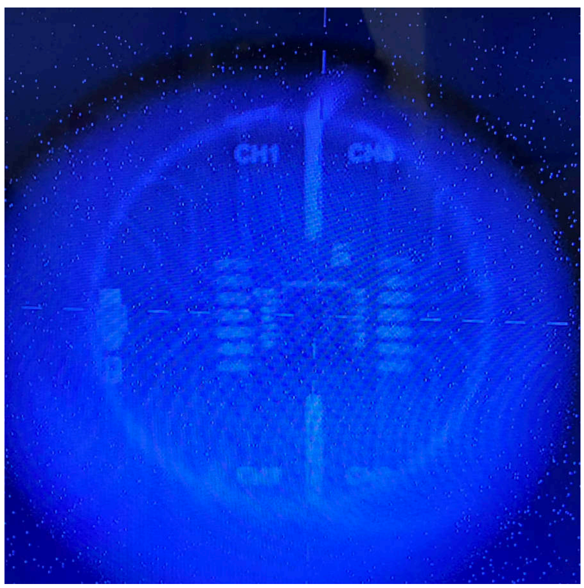

Figure 5-5. Device Under Test Lined Up With the K500 Beam

Of the two devices tested, DUT 1 was preserved for documentation purposes. DUT 2 was used for further SET characterization, in addition to two other fresh devices (DUTs 3 and 5). Each device was tested at both maximum and minimum supply voltages in a buffer circuit configuration. An input signal of V_{IN} = −1.5V was used for all tests, with the oscilloscopes set to a *window* trigger mode that captured any events where the output shifted by ±100mV or more. Each output channel was loaded with a 2kΩ resistance to GND (midsupply).

Four readpoints of 45.8MeV-cm^2 / mg, 34.5MeV-cm^2 / mg, 29.1MeV-cm^2 / mg, and 19.3MeV-cm^2 / mg were explored. The conditions for each run are summarized below. An ambient temperature of approximately 20°C was recorded in the facility at the time of these tests. See Appendix A for additional data, such as histograms.

Table 5-3. TAMU SET Characterization Run Summary

Run Number	DUT	Ion	LETeff (MeV-cm^2 /mg)	Flux (ions/s-cm^2)	Fluence (ions/cm^2)	Total Ionizing Dose (rad)	V_S (V+ − V-)	Events (Sum of All Channels)
5	2	^{109}Ag	45.8	1.135×10^5	1×10^7	36760	18	3081
6	2	^{109}Ag	45.8	1.153×10^5	9.996×10^6	36730	4.5	2453
7	5	^{109}Ag	45.8	1.077×10^5	9.997×10^6	36730	4.5	3192
8	5	^{109}Ag	45.8	1.049×10^5	1.0×10^7	36760	18	3789
9	3	^{109}Ag	45.8	9.974×10^4	1.001×10^7	36780	18	4235
10	3	^{109}Ag	45.8	1.104×10^5	1.001×10^7	36760	4.5	2865
18	3	^{84}Kr	29.1	5.347×10^5	1.000×10^7	23940	4.5	2106
19	3	^{84}Kr	29.1	5.247×10^5	9.97×10^6	23980	18	2120
20	3	^{84}Kr	34.5	5.256×10^5	9.953×10^6	23740	18	2605
21	3	^{84}Kr	34.5	5.293×10^5	9.965×10^6	23770	4.5	1957
22	2	^{84}Kr	29.1	5.349×10^5	1.002×10^7	23890	4.5	1863
23	2	^{84}Kr	29.1	5.439×10^5	1.004×10^7	23960	18	2372
24	2	^{84}Kr	34.5	5.562×10^5	1.005×10^7	23980	18	2255
25	2	^{84}Kr	34.5	5.632×10^5	1.000×10^7	23860	4.5	1905
26	5	^{84}Kr	29.1	5.464×10^5	9.978×10^6	23800	4.5	2229
27	5	^{84}Kr	29.1	5.325×10^5	9.986×10^6	23820	18	2678
28	5	^{84}Kr	34.5	5.345×10^5	9.995×10^6	23850	18	2537
29	5	^{84}Kr	34.5	5.288×10^5	1.005×10^7	23970	4.5	2217
30	5	^{63}Cu	19.3	5.240×10^5	1.004×10^7	15880	4.5	1413
31	5	^{63}Cu	19.3	4.848×10^5	1.002×10^7	15830	18	1977
32	2	^{63}Cu	19.3	4.451×10^5	9.999×10^6	15800	18	1717
33	2	^{63}Cu	19.3	3.986×10^5	9.987×10^6	15790	4.5	1437
34	3	^{63}Cu	19.3	3.458×10^5	1.001×10^7	15830	4.5	1594
35	3	^{63}Cu	19.3	3.286×10^5	1.003×10^7	15850	18	1919

Additional follow-up testing was performed using fresh devices (DUTs 6, 7, and 8). For these tests, lower-energy ions were used, to determine the transient onset point. Readpoints of 1.31MeV-cm^2 / mg, 2.68MeV-cm^2 / mg, 8.21MeV-cm^2 / mg, and 18.9MeV-cm^2 / mg were explored. The test conditions previously described were replicated for these runs.

Table 5-4. TAMU SET Follow-up Characterization Run Summary

Run Number	DUT	Ion	LETeff (MeV-cm^2 /mg)	Flux (ions/s-cm^2)	Fluence (ions/cm^2)	Total Ionizing Dose (rad)	V_S (V+ − V-)	Events (Sum of All Channels)
60	6	^{20}Ne	2.68	1.141×10^5	9.984×10^6	428	18	38
61	6	^{20}Ne	2.68	1.196×10^5	1.000×10^7	429	4.5	44
62	7	^{20}Ne	2.68	1.250×10^5	9.991×10^6	429	4.5	44
63	7	^{20}Ne	2.68	1.272×10^5	1.001×10^7	429	18	53
64	8	^{20}Ne	2.68	1.249×10^5	1.003×10^7	430	18	32
65	8	^{20}Ne	2.68	1.241×10^5	9.977×10^6	428	4.5	40
66	8	^{14}N	1.31	1.272×10^5	1.004×10^7	211	4.5	28
67	8	^{14}N	1.31	1.262×10^5	9.985×10^6	210	18	34
69	7	^{14}N	1.31	1.192×10^5	9.961×10^6	209	18	24
70	7	^{14}N	1.31	1.198×10^5	1.003×10^7	211	4.5	31
71	6	^{14}N	1.31	1.222×10^5	1.005×10^7	211	4.5	24
72	6	^{14}N	1.31	1.233×10^5	1.005×10^7	211	18	29
73	6	^{40}Ar	8.21	8.666×10^4	1.003×10^7	1320	18	119
74	6	^{40}Ar	8.21	8.832×10^4	1.002×10^7	1318	4.5	96
75	7	^{40}Ar	8.21	9.568×10^4	1.001×10^7	1316	4.5	86
76	7	^{40}Ar	8.21	9.561×10^4	1.001×10^7	1316	18	96
77	8	^{40}Ar	8.21	1.014×10^5	9.926×10^6	1310	18	116
78	8	^{40}Ar	8.21	1.001×10^5	9.979×10^6	1312	4.5	103
79	8	^{63}Cu	18.9	3.081×10^4	1.001×10^7	3036	4.5	401
80	8	^{63}Cu	18.9	2.097×10^4	9.993×10^6	3030	18	439
81	7	^{63}Cu	18.9	2.000×10^4	9.998×10^6	3032	18	477
82	7	^{63}Cu	18.9	2.132×10^4	9.997×10^6	3032	4.5	384
83	6	^{63}Cu	18.9	2.490×10^4	1.001×10^7	3035	4.5	368
84	6	^{63}Cu	18.9	2.540×10^4	1.001×10^7	3036	18	417

5.3 SEE Characterization Results: MSU FRIB Linac

For correlation purposes, two of the devices (DUT 3 and DUT 5) previously tested at TAMU were re-tested for SEL and SET at MSU's FRIB. The die temperature was held at 125°C as the units were exposed to an ion stream of ^{129}Xe, for a nominal surface LET of 50.4MeV-cm^2 / mg (Bragg peak approximately 69.3MeV-cm^2 / mg). A nominal flux of 10^5 ions / s-cm^2 was used, with each run concluding once a fluence of 10^7ions / cm^2 was reached. A latch-up was not observed for either DUT.

Testing was performed for each device in unity gain at both minimum and maximum rated supply voltage. Additionally, testing was repeated for each device at room temperature. For all testing, the outputs were observed with oscilloscope cards and transient events were recorded. An input signal of 1V was applied to all channels, with scope window thresholds set at 0.9V and 1.1V. Each output channel was loaded with a 2kΩ resistor to GND (midsupply). See Appendix B for additional data, such as histograms and plots of supply current.

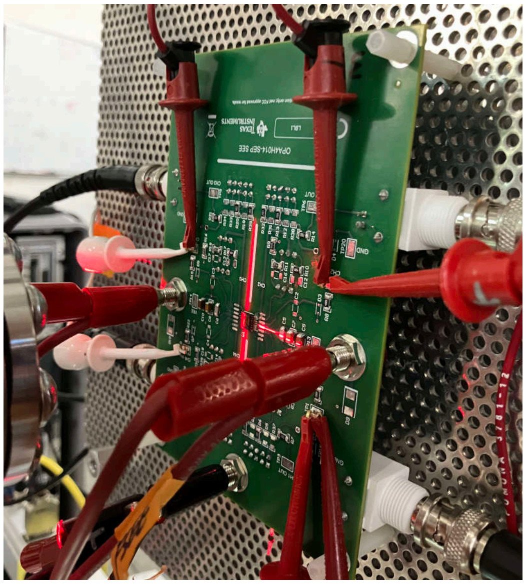

Figure 5-6. Board Mounted

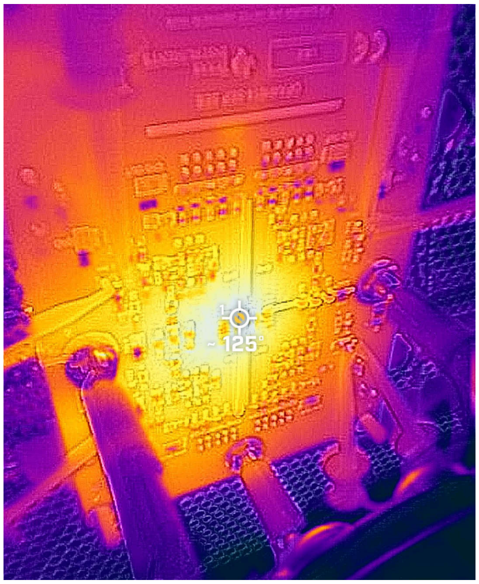

Figure 5-7. Thermal Camera

Table 5-5. MSU SEE Characterization Run Summary

Run Number	DUT	Die Temperature (°C)	Ion	LETeff (MeV-cm^2 /mg)	Flux (Ions/s-cm^2)	Fluence (Ions/cm^2)	Total Ionizing Dose (rad)	V_S (V+ − V-)	Events (Sum of All Channels)
129	3	125	^{129}Xe	50.4	1.010×10^5	1.003×10^7	8091	4.5	2004
130	3	125	^{129}Xe	50.4	1.010×10^5	1.001×10^7	8079	18	809
131	3	25	^{129}Xe	50.4	1.010×10^5	1.008×10^7	8137	18	645
132	3	25	^{129}Xe	50.4	1.010×10^5	1.006×10^7	8119	4.5	1785
133	5	125	^{129}Xe	50.4	1.010×10^5	1.001×10^7	8088	4.5	1882
134	5	125	^{129}Xe	50.4	1.010×10^5	9.999×10^6	8080	18	793
135	5	25	^{129}Xe	50.4	1.010×10^5	1.007×10^7	8135	18	755
136	5	25	^{129}Xe	50.4	1.010×10^5	1.008×10^7	8149	4.5	1766

The data supports the conclusion that the OPA4H014-SEP is robust against SEL to the maximum recommended supply voltage (18V) when exposed to heavy ions up to 50LETeff (MeV-cm^2 / mg). Testing with the die at 125°C was observed to yield higher (10% on average) event counts per run than testing at ambient temperatures.

5.4 Analysis

Information in this section describes general characteristics of the SET response characteristics of the device, and may not be accurate for all use cases or conditions. In-circuit results vary according to application specifics. TI's customers are responsible for determination of components for their purposes, and validating and testing design implementation to confirm system functionality.

The data suggest the rate at which the OPA4H014-SEP exhibits SET events, and the magnitude of those events, is a function of several factors. These include supply voltage, output loading, beam flux, ion energy, and temperature. Signal voltages, gain, and noise bandwidth are theorized as potential secondary contributors. No op-amp channel was observed to be significantly "better" or "worse", in terms of transient count, than any other. Differences in event count channel-to-channel were largely caused by differences in the oscilloscope cards used, as verified through A↔B site swaps. The output exhibited a higher tendency to shift towards the high supply rail than to the low supply rail.

Generally, when the OPA4H014-SEP experiences an SET, the output typically shifts (but not always) towards the high supply rail. These events appear as sudden *spikes* and are usually resolved within 10µs of the trigger event. Events where the output shifted by more than ±100mV were recorded by the oscilloscope cards. A small percentage of these captures show measurable undershoot or overshoot behavior after the initial spike as the output settles. Some instances of the output ringing (whether due to noise or to an SET) were also recorded. Appendix A and Appendix B show notable oscilloscope captures.

Note that the OPA4H014-SEP also experiences transient events of less than 100mV. These most likely dominate event counts, but are more difficult to measure accurately. As a result, this study focuses on only events more than 100mV in magnitude. Testing at MSU and TAMU has shown that the beam area is an electrically noisy environment, which can lead to false trigger events. Implementing filters on the device to reject noise can lead to reductions in SET count or impact the magnitude of those events. As a result, the device was tested with the full noise gain-bandwidth to serve as a worst-case analysis.

Half of the devices evaluated were tested with ion energy in *descending* order, from 45.8MeV-cm^2 / mg to 19.3MeV-cm^2 / mg. The other devices were tested with ion energy in largely *ascending* order, from 2.68MeV-cm^2 / mg to 18.9MeV-cm^2 /mg. The event counts per device as the two groups approach the same nominal LETeff differs significantly. Two possible mechanisms (not mutually exclusive) are proposed to explain this.

Table 5-6. Sum of Event Counts Per Device

LET (MeV-cm^2 /mg)	DUT 2, 4.5V	DUT 2, 18V	DUT 3, 4.5V	DUT 3, 18V	DUT 5, 4.5V	DUT 5, 18V	DUT 6, 4.5V	DUT 6, 18V	DUT 7, 4.5V	DUT 7, 18V	DUT 8, 4.5V	DUT 8, 18V
50.4	N/A	N/A	1785	645	1766	755	N/A	N/A	N/A	N/A	N/A	N/A
45.8	2453	3081	2865	4235	3192	3789	N/A	N/A	N/A	N/A	N/A	N/A
34.5	1905	2255	1957	2605	2217	2537	N/A	N/A	N/A	N/A	N/A	N/A
29.1	1863	2372	2106	2120	2229	2678	N/A	N/A	N/A	N/A	N/A	N/A
19.3	1437	1717	1594	1919	1413	1977	N/A	N/A	N/A	N/A	N/A	N/A
18.9	N/A	N/A	N/A	N/A	N/A	N/A	368	417	384	477	401	439
8.21	N/A	N/A	N/A	N/A	N/A	N/A	96	119	86	96	103	116
2.68	N/A	N/A	N/A	N/A	N/A	N/A	44	38	44	53	40	32
1.31	N/A	N/A	N/A	N/A	N/A	N/A	24	29	31	24	28	34

The first hypothesis attributes this change to differences in ion flux per run. While all runs continued until the same nominal fluence of 1 × 10^7 ions / cm^2, some runs used higher or lower flux rates than the nominal 1 × 10^5 ions/s-cm^2. A correlation between high flux rates and a high event count per device, per run can be inferred from the data. Due to facility limitations, the second group of devices were mostly tested around 2 × 10^4 ions / s-cm^2 for the copper ion. In comparison, the first group of devices saw a flux of 3.2-5.2 × 10^4 ions / s-cm^2, correlating with higher event counts. This hypothesis implies that as flux rate increases, the susceptibility of the device to SETs also increases.

The second hypothesis attributes the change to cumulative total ionizing dose (TID) damage. The OPA4H014-SEP is specified to 30krad(Si), and characterized to 50krad(Si), for high-dose-rate (HDR) TID. However, the devices used in this testing were exposed to far higher accumulated dosages. By the conclusion of testing DUT 3 experienced approximately 100krad(Si), and DUTs 3 and 5 experienced 117krad(Si). The devices were still functional despite the high stress, but showed higher event counts for copper ions than the subset of devices tested in *ascending* order. Those devices experienced approximately 5krad(Si) and experienced relatively fewer transient events. A possible link between accumulated TID damage and SET susceptibility has not been previously explored. This hypothesis implies that as more TID damage is accumulated over an operational lifetime of a device, the susceptibility to SETs increases.

Note that other factors such as the time between decap and testing (time the die is exposed to air), annealing time between runs, and simple device-to-device variation can also play a potential role in the differing event counts. Isolating any single factor is difficult due to the complexities and practical challenges of the testing.

Table 5-7. Transient Event Summary for 4.5V Supply

LET (MeV-cm^2 /mg)	50.4	45.8	34.5	29.1	19.3	18.9	8.21	2.68	1.31
Total events	3551	8510	6079	6198	4444	1153	285	128	83
Mean events per run	1775.5	2836.67	2026.33	2066	1481.33	384.33	95	42.67	27.67
Highest shift magnitude (V)	1.2044214	3.1757133	2.3809093	2.342613	1.3277632	1.4514454	1.0719484	0.9301200	0.8351200S
Lowest shift magnitude (V)	-3.1871039	-0.7210846	-0.7019365	-0.7019365	-0.6827884	-0.7306622	-0.6832251	-0.6228800	-0.6558800
Average high-going shift (V)	0.2182390	0.4619833	0.3968201	0.404437	0.3672284	0.4981227	0.5132827	0.5560549	0.4546950
Average low-going shift (V)	-0.2645667	-0.331676	-0.3146224	-0.3294971	-0.2926101	-0.3733568	-0.3094549	-0.3258800	-0.5842134
Percent of high-going events (%)	53.00	88.31	88.62	88.34	87.44	89.85	87.72	96.09	96.39

Table 5-8. Transient Event Summary for 18V Supply

LET (MeV-cm^2 /mg)	50.4	45.8	34.5	29.1	19.3	18.9	8.21	2.68	1.31
Total events	1400	11105	7397	7170	5613	1333	331	123	87
Mean events per run	700	3701.67	2465.67	2390	1871	444.33	110.33	41	29
Highest shift magnitude (V)	4.9410947	4.4020199	4.4020199	3.6638326	2.0426682	1.8783795	1.6886310	1.3621120	1.4511200
Lowest shift magnitude (V)	-3.8884764	-1.4019905	-1.4019905	-1.4019905	-1.4019905	-2.4305449	-1.0168800	-0.9998800	-0.8118800
Average high-going shift (V)	0.3026551	0.5325136	0.4420902	0.4496224	0.4070247	0.5791539	0.57418954	0.5927047	0.4427595
Average low-going shift (V)	-0.4870839	-0.3142422	-0.3912384	-0.3606623	-0.3689282	-0.4413021	-0.3800644	-0.5984800	-0.8118800
Percent of high-going events (%)	85.57	67.67	72.83	91.23	91.68	91.30	75.53	95.93	98.85

5.5 Weibull Fit

Weibull-Fit and cross section plots for the OPA4H014-SEP at supply voltages of 4.5V and of 18V are shown in Figure 5-8 and Figure 5-9, respectively. The Weibull equation used for the fits is shown in Equation 2, and the parameters used to plot the Weibull fits are provided in Table 5-11. For each of the supply voltages, the total number of transients and the run fluences are used to calculate the mean (σ_{MEAN}), upper bound (σ_{UB}), and lower bound (σ_{LB}) cross section (as discussed in Appendix C) at 95% confidence interval. Note that events recorded at MSU were not included in these calculations. As events were still recorded as low as 1.31MeV-cm^2 / mg, SET onset is assumed to fall between that point and 0MeV-cm^2 / mg. For the calculations below, onset was modeled as 0MeV-cm^2 / mg.

$$\sigma = \sigma_{SAT} \times \left(1 - e^{\left(\frac{LET - Onset}{w}\right)^{s}}\right) \tag{2}$$

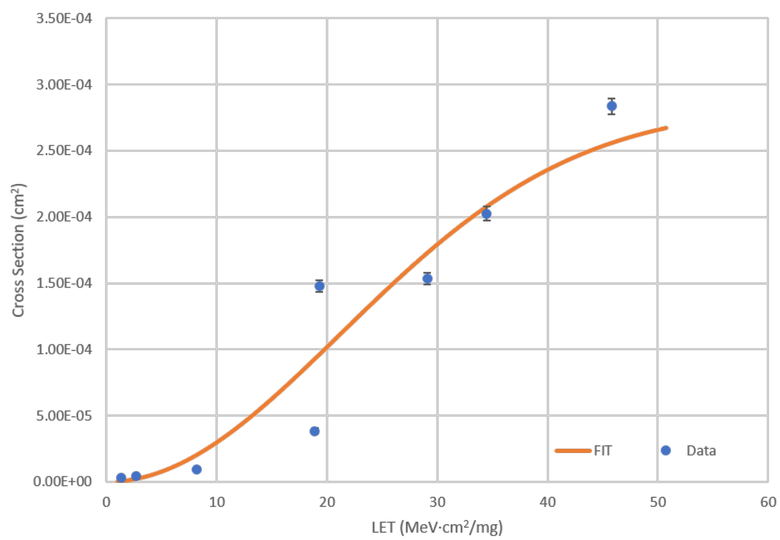

Figure 5-8. Cross Section and Weibull Fit for 4.5V Supply

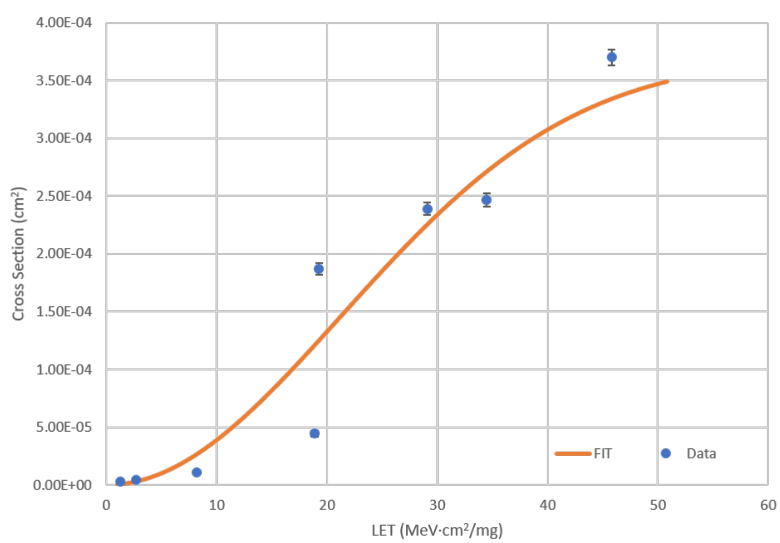

Figure 5-9. Cross Section and Weibull Fit for 18V Supply

Table 5-9. Cross Section and Weibull Fit Data: 4.5V Supply

Energy (MeV-cm^2 /mg)	Ion	Fluence (Ions/ cm^2)	Total Events	σ_{LB} (cm^2/ Device)	σ_{MEAN} (cm^2/ Device)	FIT	Residual	Residual^2	σ_{UB} (cm^2/ Device)	UB Error	LB Error
45.8	^{109}Ag	3.00E+07	8510	0.000277 644	2.84E-04	0.000256	2.76E-05	7.61E-10	2.90E-04	6.09E-06	5.99E-06
34.5	^{84}Kr	3.00E+07	6079	0.000197 472	2.03E-04	0.000208	-5.53E-06	3.05E-11	2.08E-04	5.16E-06	5.06E-06
29.1	^{84}Kr	3.00E+07	4595	0.000148 78	1.53E-04	0.000173	-1.98E-05	3.91E-10	1.58E-04	4.49E-06	4.40E-06
19.3	^{63}Cu	3.00E+07	4444	0.000143 633	1.48E-04	9.61E-05	5.18E-05	2.69E-09	1.52E-04	4.42E-06	4.32E-06
18.9	^{63}Cu	3.00E+07	1153	3.62261E-05	3.84E-05	9.29E-05	-5.45E-05	2.97E-09	4.07E-05	2.28E-06	2.19E-06
8.21	^{40}Ar	3.00E+07	285	8.42644E-06	9.50E-06	2.05E-05	-1.10E-05	1.2E-10	1.07E-05	1.17E-06	1.07E-06
2.68	^{20}Ne	3.00E+07	128	3.56338E-06	4.27E-06	2.25E-06	2.02E-06	4.07E-12	5.08E-06	8.07E-07	7.08E-07
1.31	^{14}N	3.01E+07	83	2.19486E-06	2.76E-06	5.4E-07	2.22E-06	4.91E-12	3.42E-06	6.60E-07	5.61E-07

Table 5-10. Cross Section and Weibull Fit Data, 18V Supply

Energy (MeV-cm^2 /mg)	Ion	Fluence (Ions/ cm^2)	Total Events	σ_{LB} (cm^2/ Device)	σ_{MEAN} (cm^2/ Device)	FIT	Residual	Residual^2	σ_{UB} (cm^2 / Device)	UB Error	LB Error
45.8	^{109}Ag	3.00E+07	11105	0.000363 193	3.70E-04	0.000256	1.14E-04	1.3E-08	3.77E-04	6.95E-06	6.85E-06
34.5	^{84}Kr	3.00E+07	7397	0.000240 995	2.47E-04	0.000208	3.85E-05	1.48E-09	2.52E-04	5.68E-06	5.59E-06
29.1	^{84}Kr	3.00E+07	7170	0.000233 531	2.39E-04	0.000173	6.61E-05	4.37E-09	2.45E-04	5.60E-06	5.50E-06
19.3	^{63}Cu	3.00E+07	5613	0.000181 94	1.87E-04	9.61E-05	9.07E-05	8.22E-09	1.92E-04	4.95E-06	4.86E-06
18.9	^{63}Cu	3.00E+07	1333	4.20784E-05	4.44E-05	9.29E-05	-4.85E-05	2.35E-09	4.69E-05	2.45E-06	2.35E-06
8.21	^{40}Ar	3.00E+07	331	9.87594E-06	1.10E-05	2.05E-05	-9.43E-06	8.9E-11	1.23E-05	1.25E-06	1.16E-06
2.68	^{20}Ne	3.00E+07	123	3.40478E-06	4.10E-06	2.25E-06	1.84E-06	3.39E-12	4.89E-06	7.91E-07	6.92E-07
1.31	^{14}N	3.00E+07	87	2.32309E-06	2.90E-06	5.4E-07	2.36E-06	5.57E-12	3.58E-06	6.77E-07	5.77E-07

Table 5-11. Weibull Fit Parameters

Parameter	Value for 4.5V Supply	Value for 18V Supply
σ_{SAT} (cm^2)	2.8364×10^{-4}	3.7004×10^{-4}
Onset (MeV-cm^2 /mg)	0	0
w	30	30
s	2	2
Sum (Residual^2)	6.96746×10^{-9}	2.95133×10^{-8}

6 Summary

Single-event effects of the OPA4H014-SEP radiation tolerant, high-performance, 11MHz, low-noise, precision RRO JFET amplifier were studied. The device was shown through characterization to be latch-up immune up to surface LET_{EFF} = 50MeV-cm^2 / mg and T = 125°C, providing additional margin beyond the specified level of surface LET_{EFF} = 43MeV-cm^2/ mg and T = 125°C already proven in qualification.

A TAMU Results Appendix

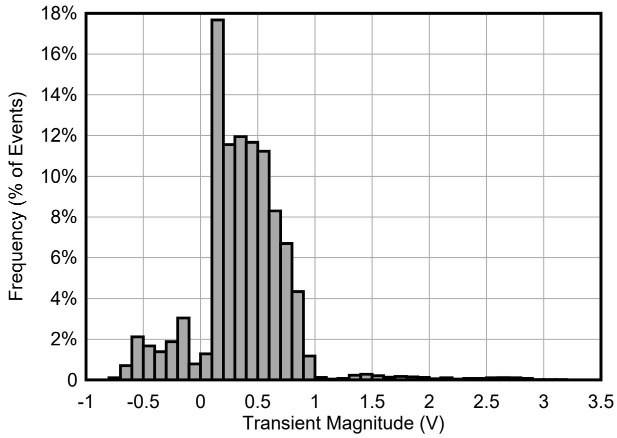

Figure A-1. Transient Event Magnitude Histogram, 4.5V Supply, LETeff = 45.8MeV-cm^2 / mg

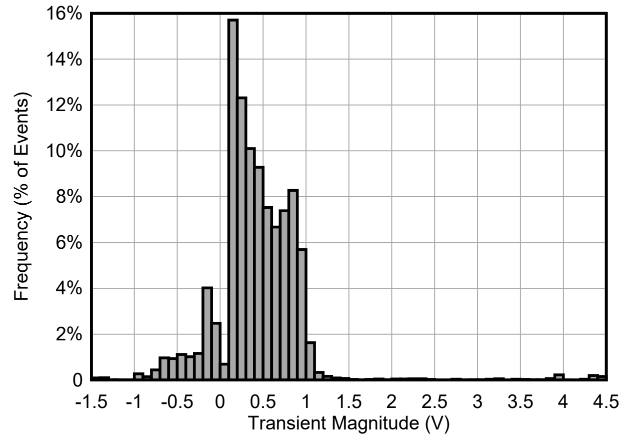

Figure A-2. Transient Event Magnitude Histogram, 18V Supply, LETeff = 45.8MeV-cm^2 / mg

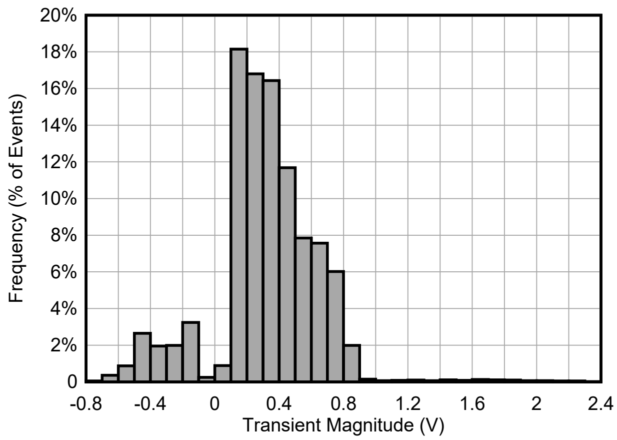

Figure A-3. Transient Event Magnitude Histogram, 4.5V Supply, LETeff = 34.5MeV-cm^2 / mg

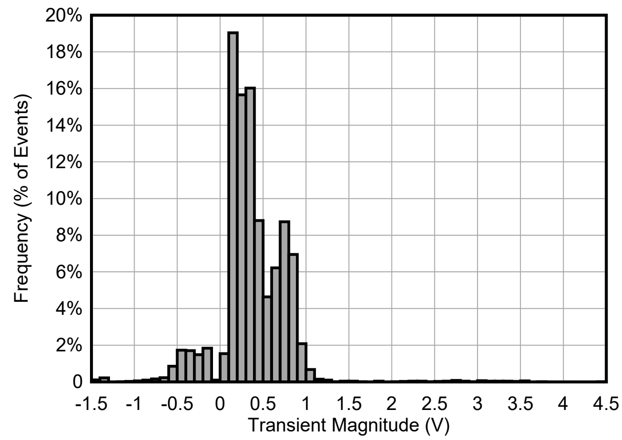

Figure A-4. Transient Event Magnitude Histogram, 18V Supply, LETeff = 34.5MeV-cm^2 / mg

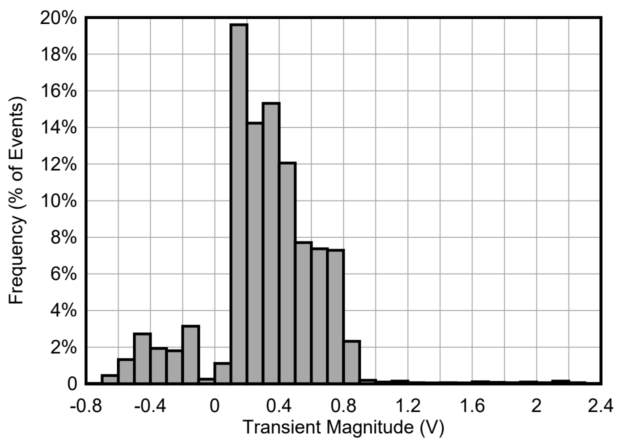

Figure A-5. Transient Event Magnitude Histogram, 4.5V Supply, LETeff = 29.1MeV-cm^2 / mg

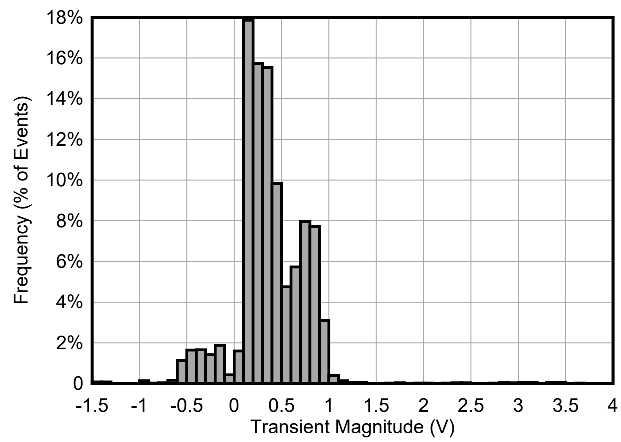

Figure A-6. Transient Event Magnitude Histogram, 18V Supply, LETeff = 29.1MeV-cm^2 / mg

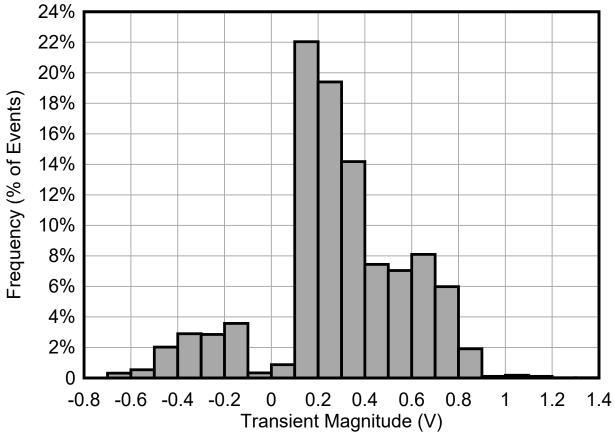

Figure A-7. Transient Event Magnitude Histogram, 4.5V Supply, LETeff = 19.3MeV-cm^2 / mg

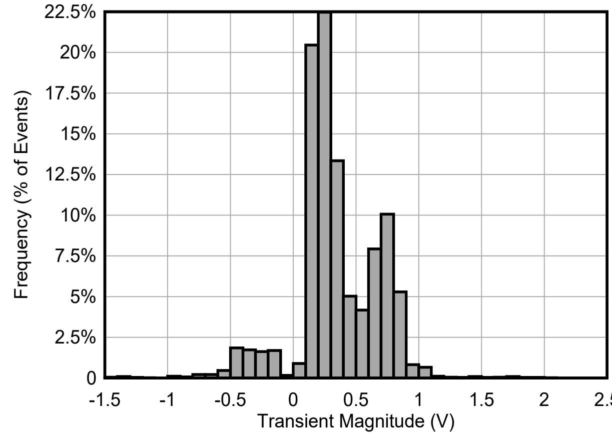

Figure A-8. Transient Event Magnitude Histogram, 18V Supply, LETeff = 19.3MeV-cm^2 / mg

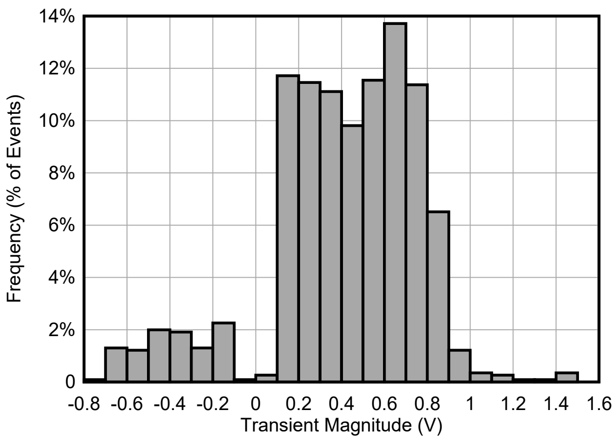

Figure A-9. Transient Event Magnitude Histogram, 4.5V Supply, LETeff = 18.9MeV-cm^2 / mg

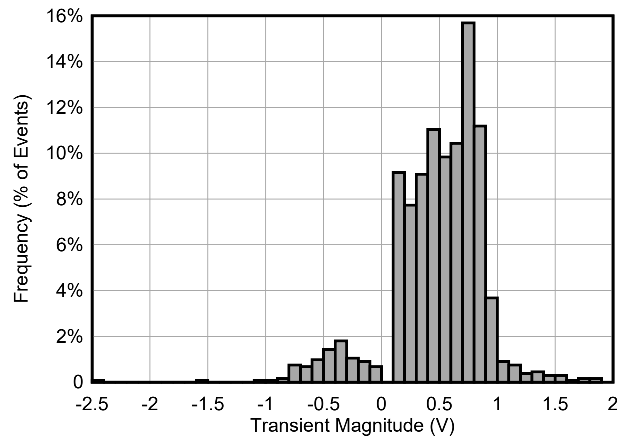

Figure A-10. Transient Event Magnitude Histogram, 18V Supply, LETeff = 18.9MeV-cm^2 / mg

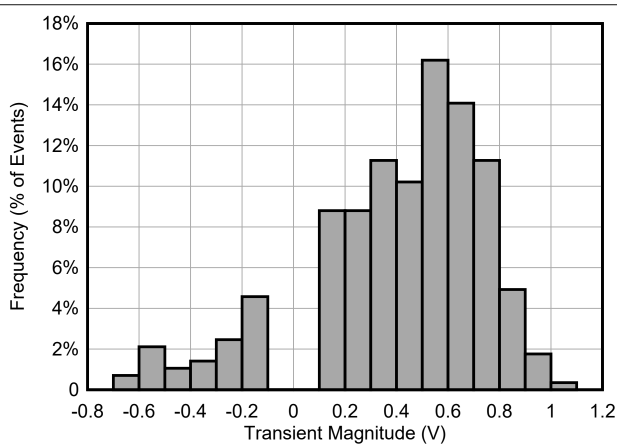

Figure A-11. Transient Event Magnitude Histogram, 4.5V Supply, LETeff = 8.21MeV-cm^2 / mg

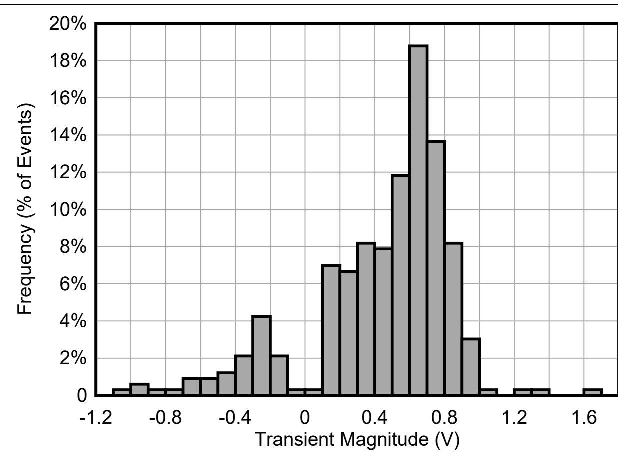

Figure A-12. Transient Event Magnitude Histogram, 18V Supply, LETeff = 8.21MeV-cm^2 / mg

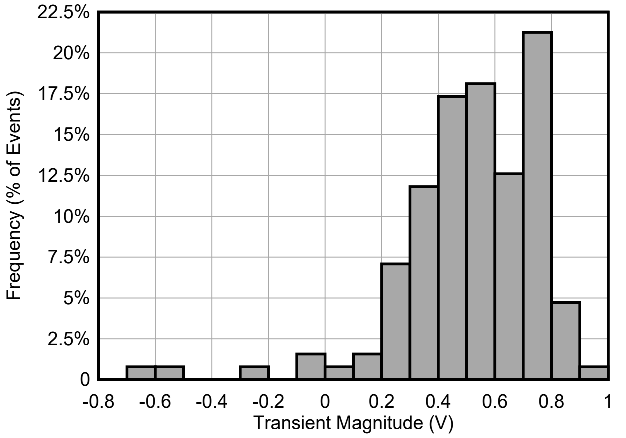

Figure A-13. Transient Event Magnitude Histogram, 4.5V Supply, LETeff = 2.68MeV-cm^2 / mg

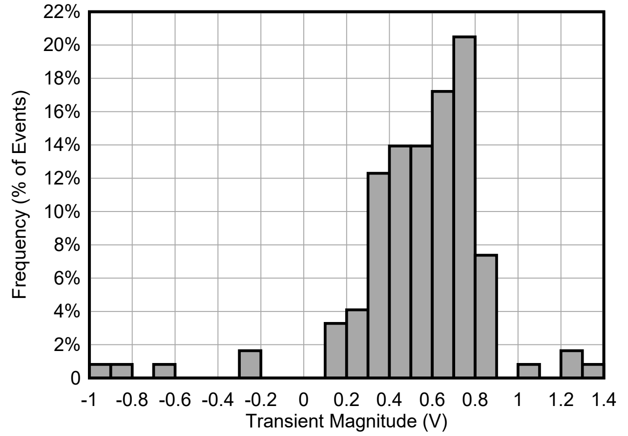

Figure A-14. Transient Event Magnitude Histogram, 18V Supply, LETeff = 2.68MeV-cm^2 / mg

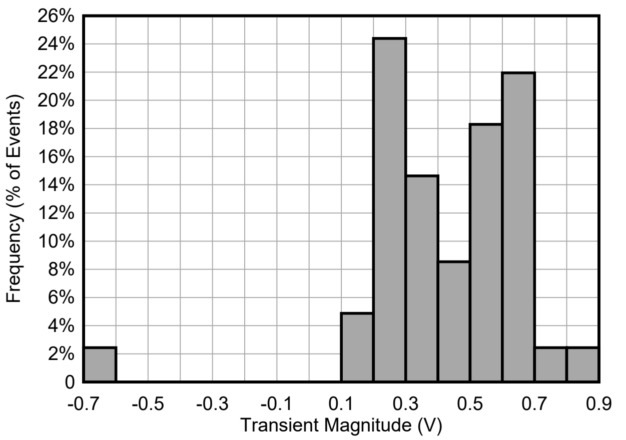

Figure A-15. Transient Event Magnitude Histogram, 4.5V Supply, LETeff = 1.31MeV-cm^2 / mg

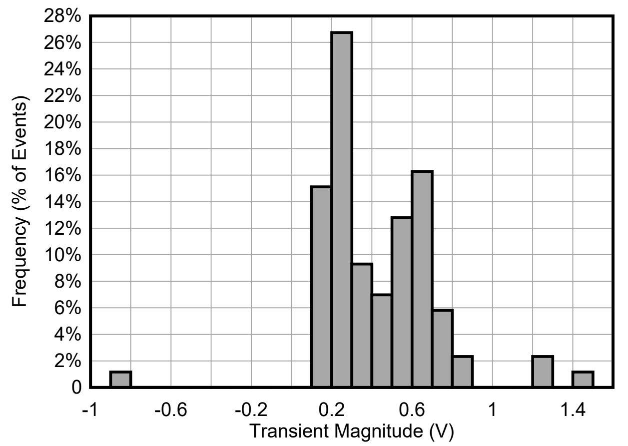

Figure A-16. Transient Event Magnitude Histogram, 18V Supply, LETeff = 1.31MeV-cm^2 / mg

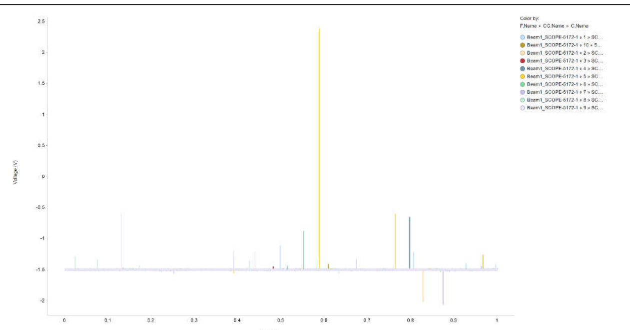

Figure A-17. TAMU Run 5, Events 1-10, SCOPE1

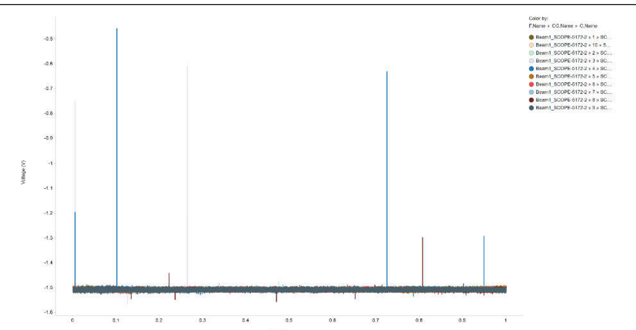

Figure A-18. TAMU Run 5, Events 1-10, SCOPE2

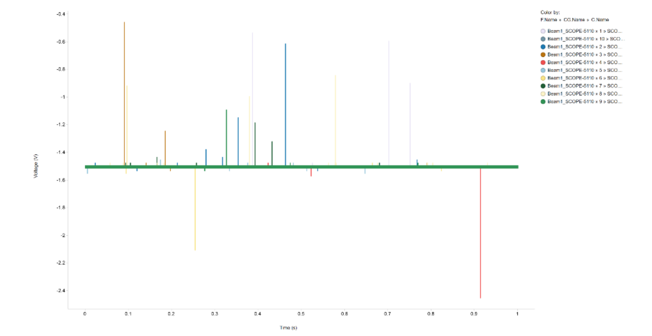

Figure A-19. TAMU Run 5, Events 1-10, SCOPE3

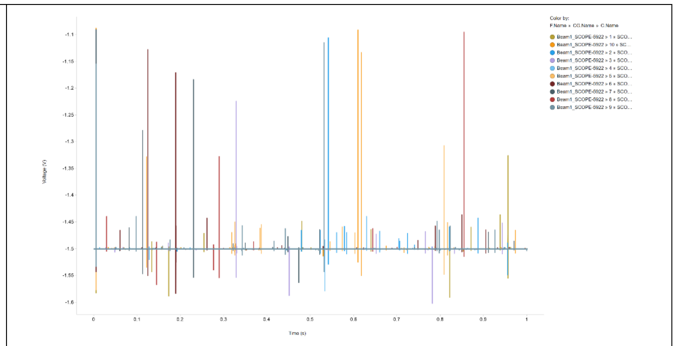

Figure A-20. TAMU Run 5, Events 1-10, SCOPE4

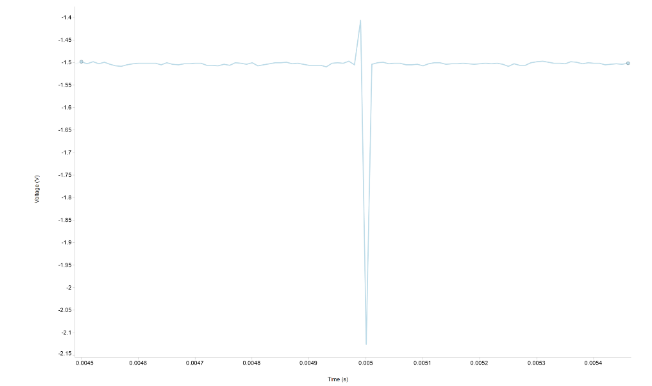

Figure A-21. TAMU Run 61, Event 13, SCOPE1

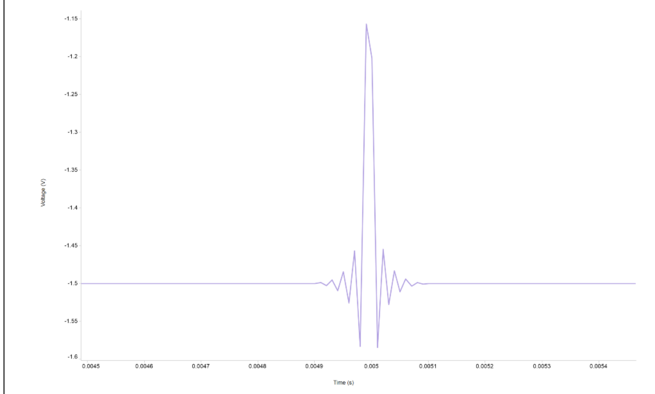

Figure A-22. TAMU Run 64, Event 3, SCOPE4

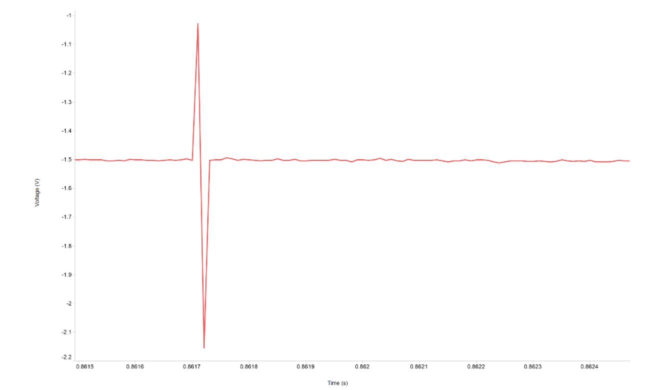

Figure A-23. TAMU Run 76, Event 46, SCOPE2

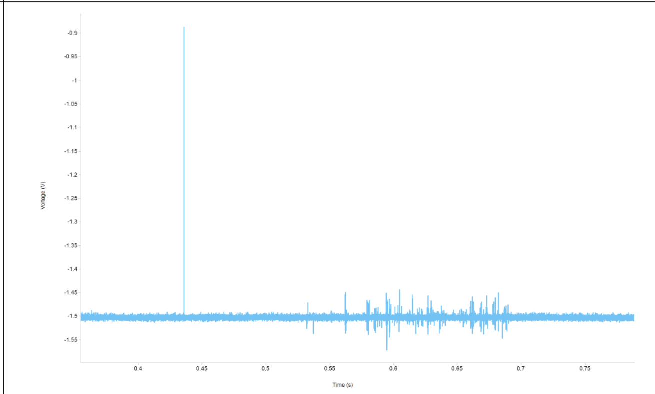

Figure A-24. TAMU Run 80, Event 182, SCOPE1

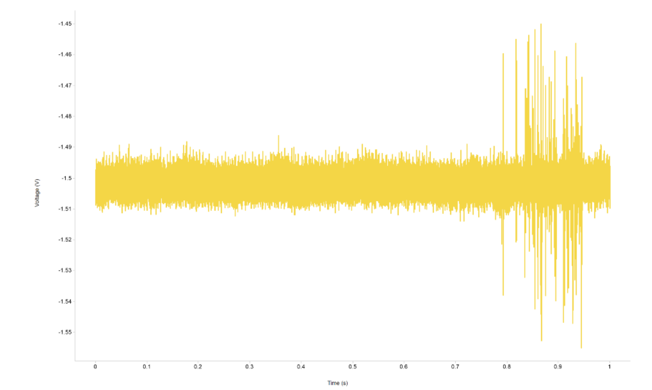

Figure A-25. TAMU Run 80, Event 182, SCOPE2

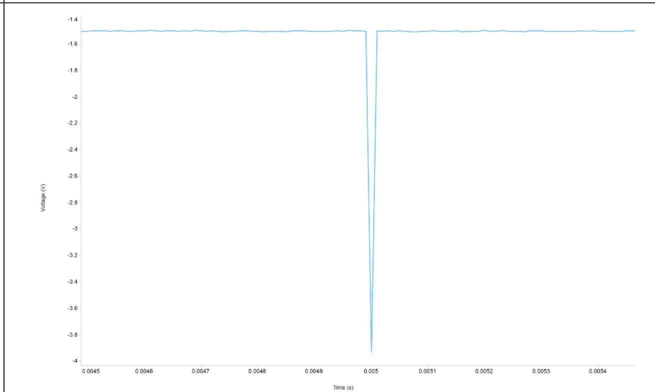

Figure A-26. TAMU Run 81, Event 45, SCOPE2

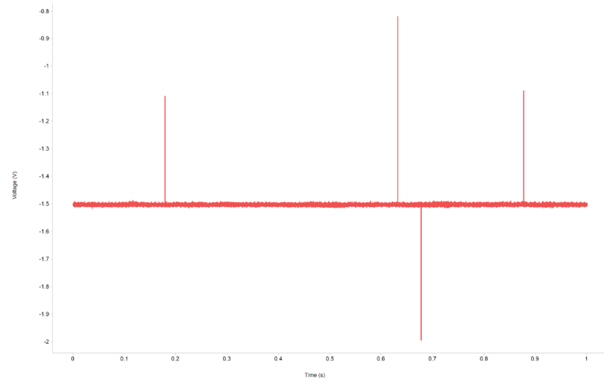

Figure A-27. TAMU Run 82, Event 158, SCOPE2

B MSU Results Appendix

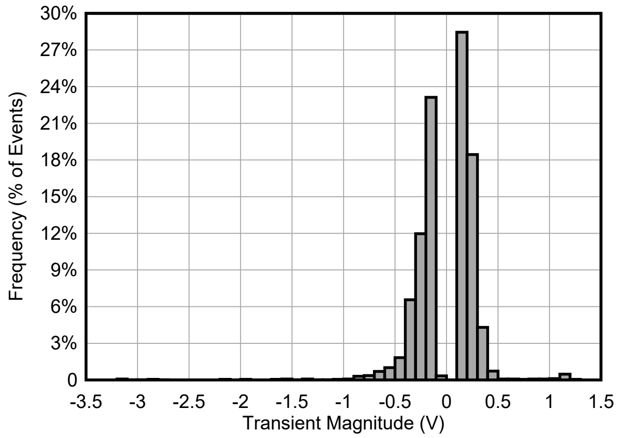

Figure B-1. Transient Event Magnitude Histogram, 4.5V Supply, LETeff = 50.4MeV-cm^2 / mg

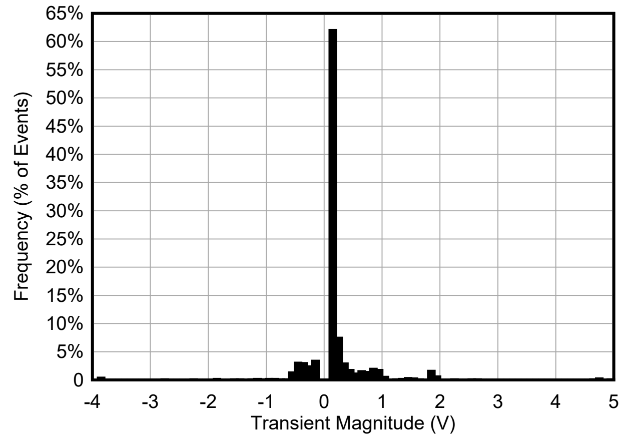

Figure B-2. Transient Event Magnitude Histogram, 18V Supply, LETeff = 50.4MeV-cm^2 / mg

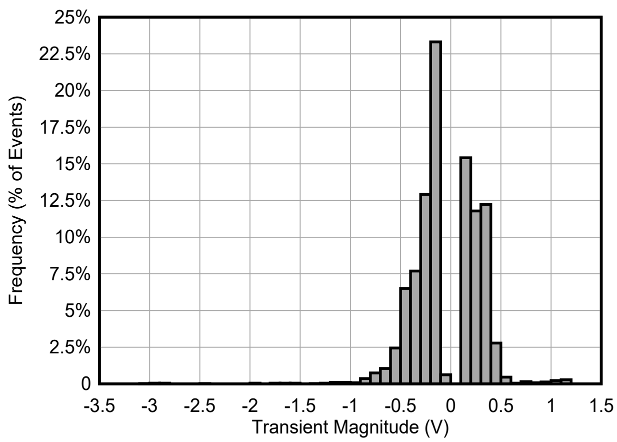

Figure B-3. Transient Event Magnitude Histogram, 4.5V Supply, LETeff = 50.4MeV-cm^2 / mg, T_J = 125°C

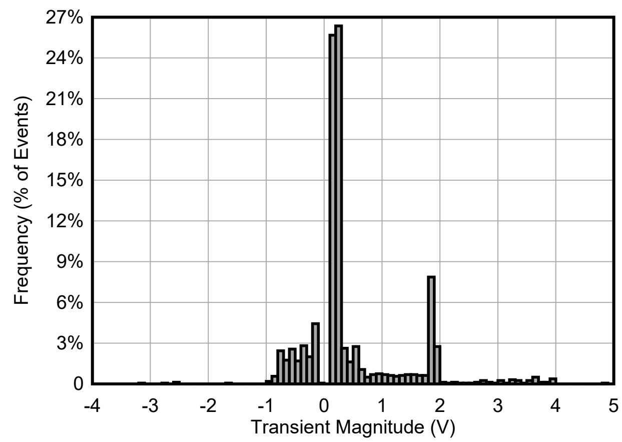

Figure B-4. Transient Event Magnitude Histogram, 18V Supply, LETeff = 50.4MeV-cm^2 / mg, T_J = 125°C

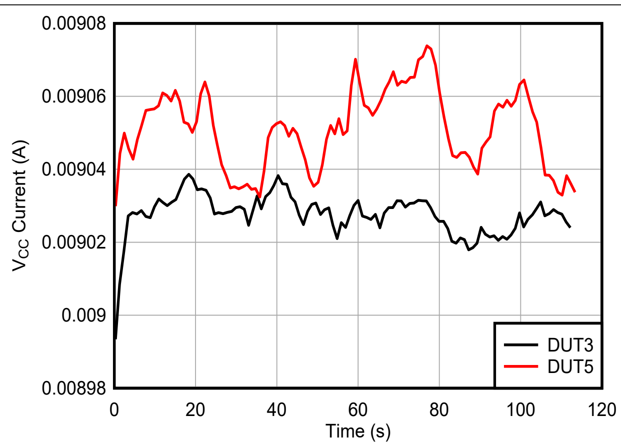

Figure B-5. VCC Supply Current, 4.5V Supply, LETeff = 50.4MeV-cm^2 / mg, T_J = 125°C

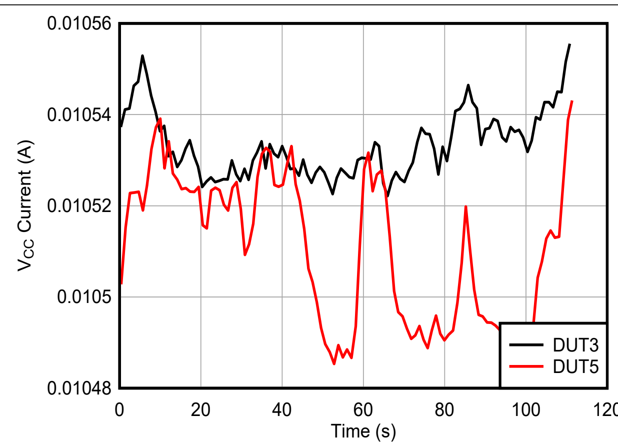

Figure B-6. VCC Supply Current, 18V Supply, LETeff = 50.4MeV-cm^2 / mg, T_J = 125°C

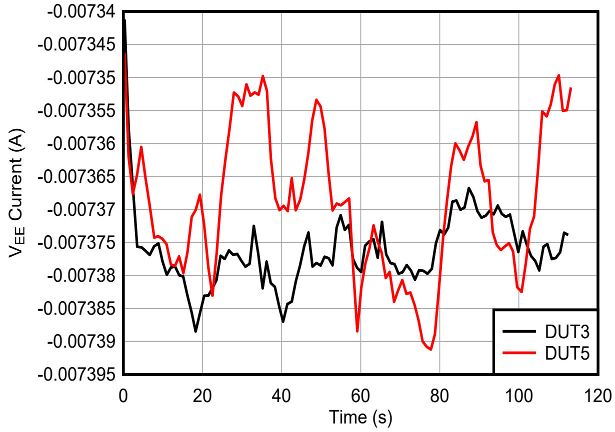

Figure B-7. VEE Supply Current, 4.5V Supply, LETeff = 50.4MeV-cm^2 / mg, T_J = 125°C

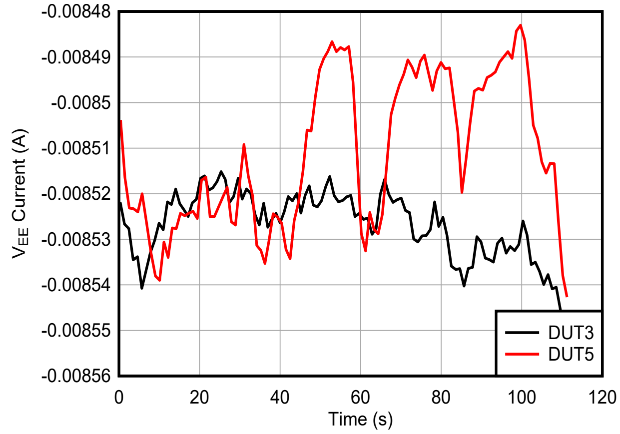

Figure B-8. VEE Supply Current, 18V Supply, LETeff = 50.4MeV-cm^2 / mg, T_J = 125°C

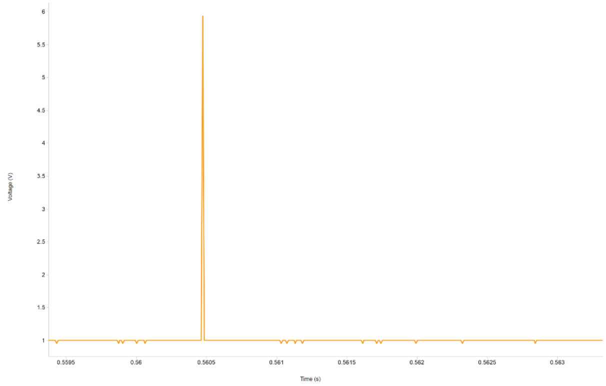

Figure B-9. MSU Run 77, Event 64, VOUT1

C Confidence Interval Calculations

For conventional products where hundreds of failures are seen during a single exposure, one can determine the average failure rate of parts being tested in a heavy-ion beam as a function of fluence with high degree of certainty and reasonably tight standard deviation, and as a result, have confidence that the calculated cross-section is accurate.

With radiation-hardened parts however, it is difficult to determine the cross-section because often few or no failures are observed during an entire exposure. Determining the cross-section using an average failure rate with standard deviation is no longer a viable option, and the common practice of assuming a single error occurred at the conclusion of a null-result can result in a greatly underestimated cross-section.

In cases where observed failures are rare or non-existent, the use of confidence intervals and the chi-squared distribution is indicated. The chi-squared distribution is particularly designed for the determination of a reliability level when the failures occur at a constant rate. In the case of SEE testing where the ion events are random in time and position within the irradiation area, a failure rate is expected that is independent of time (presuming that parametric shifts induced by the total ionizing dose do not affect the failure rate), and as a result, the use of chi-squared statistical techniques is valid (because events are rare, an exponential or Poisson distribution is used).

In a typical SEE experiment, the device-under-test (DUT) is exposed to a known, fixed fluence (ions / cm^2) while the DUT is monitored for failures. This is analogous to fixed-time reliability testing and, more specifically, time-terminated testing where the reliability test is terminated after a fixed amount of time whether or not a failure has occurred (in the case of SEE tests fluence is substituted for time and hence it is a fixed fluence test [(6)]). Calculating a confidence interval specifically provides a range of values which is likely to contain the parameter of interest (the actual number of failures per fluence). Confidence intervals are constructed at a specific confidence level. For example, a 95% confidence level implies that if a given number of units were sampled numerous times and a confidence interval estimated for each test, the resulting set of confidence intervals can bracket the true population parameter in about 95% of the cases.

To estimate the cross-section from a null-result (no fails observed for a given fluence) with a confidence interval, start with the standard reliability determination of lower-bound (minimum) mean-time-to-failure for fixed-time testing (an exponential distribution is assumed) in Equation 3:

$$MTTF = \frac{2nT}{\chi^2_{2(d+1);\,100\left(1-\frac{\alpha}{2}\right)}} \tag{3}$$

Where:

- *MTTF* is the minimum (lower-bound) mean-time-to-failure,
- *n* is the number of units tested (presuming each unit is tested under identical conditions),
- *T* is the test time,
- and χ^2 is the chi-square distribution evaluated at 100(1 – α / 2) confidence level
- *d* is the degrees-of-freedom (the number of failures observed).

With slight modification for our purposes we invert the inequality and substitute *F* (fluence) in the place of *T* as shown in Equation 4:

$$MFTF = \frac{2nF}{\chi^2_{2(d+1);\,100\left(1-\frac{\alpha}{2}\right)}} \tag{4}$$

Where:

- *MFTF* is mean-fluence-to-failure
- *F* is the test fluence
- X^2 is the chi-square distribution evaluated at 100(1 – α / 2) confidence
- *d* is the degrees-of-freedom (the number of failures observed).

The inverse relation between *MTTF* and failure rate is mirrored with the *MFTF*. Thus the upper-bound cross-section is obtained by inverting the *MFTF* as shown in Equation 5:

$$\sigma = \frac{\chi^2_{2(d+1);100\left(1-\frac{\alpha}{2}\right)}}{2nF} \tag{5}$$

Assume that all tests are terminated at a total fluence of 10^6 ions/cm^2. Assume there are a number of devices with different performances that are tested under identical conditions. Assume a 95% confidence level (σ = 0.05). Note that as *d* increases from 0 events to 100 events, the actual confidence interval becomes smaller, which indicates that the range of values of the true value of the population parameter (in this case, the cross-section) is approaching the mean value + 1 standard deviation. As more events are observed, the statistics are improved such that uncertainty in the actual device performance is reduced.

Table C-1. Experimental Example Calculation of MFTF and σ Using a 95% Confidence Interval(1)

Degrees-of-Freedom (d)	2(d + 1)	X^2 at 95%	Calculated Cross-Section (cm^2)		
			Upper-Bound at 95% Confidence	Mean	Average + Standard Deviation
0	2	7.38	3.69E–06	0.00E+00	0.00E+00
1	4	11.14	5.57E–06	1.00E–06	2.00E–06
2	6	14.45	7.22E–06	2.00E–06	3.41E–06
3	8	17.53	8.77E–06	3.00E–06	4.73E–06
4	10	20.48	1.02E–05	4.00E–06	6.00E–06
5	12	23.34	1.17E–05	5.00E–06	7.24E–06
10	22	36.78	1.84E–05	1.00E–05	1.32E–05
50	102	131.84	6.59E–05	5.00E–05	5.71E–05
100	202	243.25	1.22E–04	1.00E–04	1.10E–04

(1) Using a 95% confidence interval for several different observed results (d = 0, 1, 2,…100 observed events during fixed-fluence tests) assuming 10^6 ions / cm^2 for each test. Note that as the number of observed events increases the confidence interval approaches the mean.

D References

1. M. Shoga and D. Binder, Theory of Single Event Latchup in Complementary Metal-Oxide Semiconductor Integrated Circuits, *IEEE Trans. Nucl. Sci., Vol. 33(6)*, Dec. 1986, pp. 1714-1717.
2. G. Bruguier and J. M. Palau, "Single particle-induced latchup", *IEEE Trans. Nucl. Sci., Vol. 43(2)*, Mar. 1996, pp. 522-532.
3. Texas A&M University, *Texas A&M University Cyclotron Institute Radiation Effects Facility*, webpage.
4. Michigan State University, *MSU Facility for Rare Isotope Beams*, webpage.
5. Ziegler, James F. *The Stopping and Range of Ions in Matter*, webpage.
6. D. Kececioglu, “Reliability and Life Testing Handbook”, Vol. 1, PTR Prentice Hall, New Jersey, 1993, pp. 186-193.
7. Vanderbilt University, *ISDE CRÈME-MC*, webpage.
8. A. J. Tylka, J. H. Adams, P. R. Boberg, et al.,"CREME96: A Revision of the Cosmic Ray Effects on Micro-Electronics Code", *IEEE Trans. on Nucl. Sci., Vol. 44(6)*, Dec. 1997, pp. 2150-2160.
9. A. J. Tylka, W. F. Dietrich, and P. R. Boberg, "Probability distributions of high-energy solar-heavy-ion fluxes from IMP-8: 1973-1996", *IEEE Trans. on Nucl. Sci.,Vol. 44(6)*, Dec. 1997, pp. 2140-2149.

IMPORTANT NOTICE AND DISCLAIMER